Available online at www.sciencedirect.com

SciVerse ScienceDirect

Ceramics International 38 (2012) 2225–2231

CERAMICS INTERNATIONAL

www.elsevier.com/locate/ceramint

Nanostructured ferrites: Structural analysis and catalytic activity

Adriana S. Albuquerque [a,*], Marcus V.C. Tolentino [a], José D. Ardisson [a], Flávia C.C. Moura [b], Renato de Mendonça [a,c], Waldemar A.A. Macedo [a]

[a] *Laboratório de Física Aplicada, Centro de Desenvolvimento e Tecnologia Nuclear - CDTN, Belo Horizonte 31270-901, MG, Brazil*
[b] *Departamento de Química, ICEx, Universidade Federal de Minas Gerais - UFMG, 31270-901 Belo Horizonte, MG, Brazil*
[c] *REDEMAT, Escola de Minas, Universidade Federal de Ouro Preto - UFOP, 35400-000 Ouro Preto, MG, Brazil*

Received 31 January 2011; received in revised form 21 October 2011; accepted 27 October 2011
Available online 4 November 2011

Abstract

In this work, we have investigated the structural and catalytic properties of Co, Cu and Ni spinel ferrites. Nanostructured ferrites with particle diameters varying from 3 to 10 nm were obtained by the co-precipitation process. X-ray diffraction, X-ray fluorescence, X-ray photoelectron spectroscopy and Mössbauer spectroscopy were used for chemical and structural characterization. The catalytic efficiency of the samples was evaluated by the decomposition of hydrogen peroxide and by the oxidation of methylene blue, monitored via UV–vis spectrophotometry. We observed that the presence of cobalt ions is a crucial factor required to achieve a systematic efficiency of the catalyst in the H_2O_2 decomposition. In contrast, Cu ferrites presented the better performance in methylene blue oxidation, which can be attributed to the different redox properties of Cu and the easier availability of electrons to participate in the oxidation of organic compounds.

Keywords: C. Chemical properties; D. Ferrites; Nanostructures; Catalytic activity

1. Introduction

Iron oxides have well-established catalytic properties for many reactions such as decomposition of alcohols, selective oxidation of carbon monoxide, decomposition of hydrogen peroxide and discoloration of synthetic dyes, and have been extensively studied for environmental applications [1–6]. Cubic ferrites have spinel structure with the general formula $M^{2+}Fe_2^{3+}O_4$, where M^{2+} is a divalent metallic ion such as Fe^{2+}, Ni^{2+}, Cu^{2+}, Zn^{2+}, Co^{2+}. The spinel configuration is based on a face centered cubic lattice of oxygen ions, forming tetrahedral (A) and octahedral [B] coordination sites that may be occupied either by M^{2+} and/or Fe^{3+} ions. Also, mixed ferrites can be produced, in the sense that part of the M^{2+} can be isomorphically substituted and final formula may contain mixed divalent ions $(M^{2+})'_{1-x}(M^{2+})''_x(Fe^{3+})_2O_4$, allowing it possible to obtain a wide range of spinel ferrites with variable compositions [7,8]. The catalytic properties of spinels containing transition metal ions are dependent on the redox properties of substituting ions and on their distribution among the octahedral and tetrahedral coordination sites. The surface of spinel oxide powders contains mainly octahedral sites and, consequently, its catalytic activity is crucially related to the octahedral cations [9–11]. In addition to the chemical modifications, physical modifications of spinel ferrites, such as the decrease of the particle size by milling or by selecting a particular route of synthesis, have been reported to increase the catalytic performance of these materials [12]. The preparation of nanopowder ferrites with controlled chemical structure, crystallite size and crystallite size distribution, can be obtained from the co-precipitation method described in a previous publication [13].

In this work, we investigate the chemical and structural properties of pure Co-, Cu- and Ni-spinel ferrites and along with mixed (Co, Cu)-, (Cu, Ni)- and (Co, Ni)-spinel ferrites obtained by the coprecipitation method, and the catalytic activity of these materials on the oxidation an organic probe molecule, namely methylene blue. The chemical and structural characterizations of the ferrites powder were made with X-ray diffraction (XRD), X-ray fluorescence (XRF), Mössbauer spectroscopy (MS) and X-ray photoelectron spectroscopy (XPS). The catalytic

* Corresponding author. Tel.: +55 31 3069 3196; fax: +55 31 3069 3390.
E-mail address: asa@cdtn.br (A.S. Albuquerque).

0272-8842/$36.00
doi:10.1016/j.ceramint.2011.10.071

efficiency of the samples was evaluated by both, the decomposition of H_2O_2 and the oxidation of methylene blue in aqueous medium.

2. Experimental

The ferrite samples were synthesized by the co-precipitation method using Fe, Cu, Co and Ni nitrates (Synth) dissolved in given stoichiometric proportions in deionized water to obtain the corresponding ferrites $CoFe_2O_4$, $CuFe_2O_4$, $NiFe_2O_4$, $Co_{0.5}Cu_{0.5}Fe_2O_4$, $Co_{0.5}Ni_{0.5}Fe_2O_4$, and $Cu_{0.5}Ni_{0.5}Fe_2O_4$. After stirring, it was added the nitrates solution on a solution containing precipitating agent NaOH (3.5 M). The resulting precipitate was filtered, washed with deionized water and acetone, and dried at 70 °C for 24 h. The powder so obtained was submitted to thermal annealing at 400 °C during 2 h, in air. The ferrite samples were characterized by X-ray diffraction using a Geigerflex Rigaku diffractometer (Cu Kα radiation), X-ray fluorescence (Shimadzu EDX-720) and Transmission ^{57}Fe Mössbauer measurements, done at 25 K, on a constant acceleration estimate with a ^{57}Co/Rh source. The Normos least-square fitting package was used in order to estimate the hyperfine parameters. XPS analysis was conducted with a non-monochromatic Mg Kα X-ray source ($h\nu$ = 1253.6 eV) and a hemispherical concentric analyzer (CLAM2 – VG Microtech). The binding energies were corrected through C (1s) reference peak at 284.6 eV. The H_2O_2 (30%, v/v, Synth) decomposition was carried out using a 7 mL H_2O_2 solution (2.9 mol L^{-1}) and 30 mg of ferrite, monitoring the resulting O_2 in a volumetric glass system [12]. In order to study the oxidation of methylene blue (2.0 ml of a solution 0.1 g L^{-1}), 2 mL of H_2O_2 and 30 mg of nanopowder ferrite were added to the aqueous solution, under stirring. The oxidation reaction was monitored via UV–vis measurements at λ = 665 nm (Shimadzu-UV-1601 PC). The solution of hydrogen peroxide was added only after the first absorbance measurement was made. The efficiency of the catalysts was evaluated through the oxidation (discoloration) kinetics of methylene blue.

3. Results and discussion

3.1. Characterization of the ferrites

The X-ray diffraction patterns for Co-, Cu-, Ni-, (CoCu)-, (CuNi)- and (CoNi)-ferrites suggested the presence of cubic spinel phases, as indicated by the (1 1 1), (2 2 0), (3 1 1), (2 2 2), (4 0 0), (4 2 2), (5 1 1) and (4 4 0) reflection peaks. The position and relative intensity of all diffraction peaks for these samples, shown in Fig. 1, are in close agreement with the standard diffraction data (JCPDS card no. 22-1086, 03-0875 and 25-0283, for cobalt, nickel and copper ferrite, respectively) and previous reports [14–17]. The broad width of the peaks is indicative of low crystallinity and the strong nanostructural dimensions of the samples.

The crystallite sizes, which vary from 3 to 10 nm (Table 1), were calculated from the X-ray peak broadening of (3 1 1) diffraction peak using the Scherrer equation. The unit cell

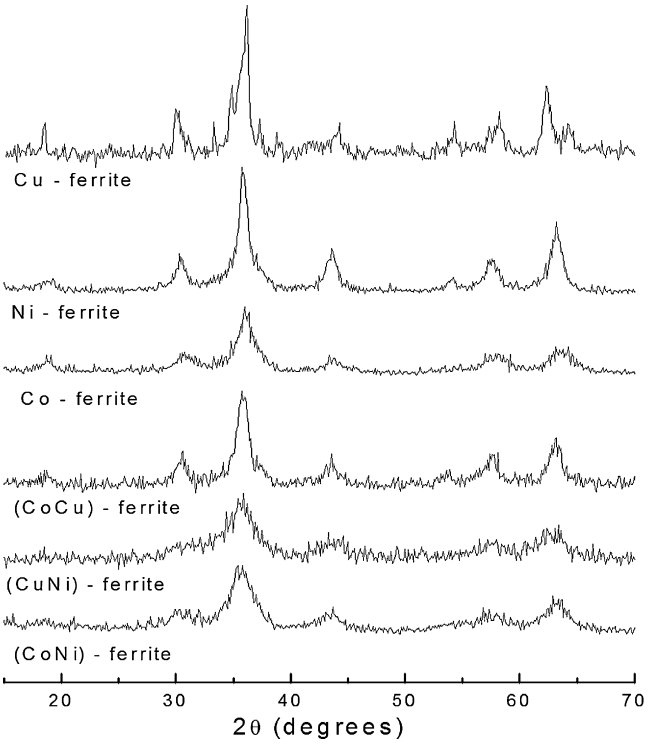

Fig. 1. X-ray diffraction patterns of the different nanosized spinel ferrites.

parameters, estimated by using interplanar spacing, for these cubic nanoparticles ferrites vary from 8.28 to 8.34 Å, while that presented in JCPDS cards for corresponding well crystallized cubic ferrites vary from 8.34 to 8.40 Å. The smaller a values observed for our samples can be associated to their low crystalline quality and similar results were reported for nanostructured ferrites [18–20]. X-ray fluorescence indicated the following spinel ferrites composition: $Co_{0.93}Fe_{2.08}O_4$, $Cu_{0.94}Fe_{2.06}O_4$, $Ni_{1.05}Fe_{1.95}O_4$, $Co_{0.35}Cu_{0.67}Fe_{1.98}O_4$, $Co_{0.46}Ni_{0.64}Fe_{1.90}O_4$, and $Cu_{0.40}Ni_{0.50}Fe_{2.10}O_4$.

Mössbauer spectra obtained at 25 K for all the ferrospinels samples, that are shown in Fig. 2, were fitted with two sextets, corresponding to Fe^{3+} ions located in tetrahedral (A) and octahedral [B] sites [21,22]. The distribution of cations in this type of structure may be described as $(M_xFe_{1-x})[M_{1-x}Fe_{1+x}]O_4$, being x the inversion parameter, whose value is among 0–1, for normal and inverse spinel respectively [8,14]. The resulting Mössbauer parameters are presented in the Table 1, which gives values of isomer shift relative to α-Fe (δ), quadrupole splitting (ξ), magnetic hyperfine field (BHF), and proportional area corresponding to Fe^{3+} ions in percentage, in tetrahedral sites (A) and in octahedral sites [B]. The higher value of hyperfine fields was assigned to the Fe^{3+} in octahedral sites whereas the lower value was related to Fe^{3+} in tetrahedral sites. The hyperfine values obtained are coherent with the literature for spinel Co-, Cu- and Ni-ferrites [14,21] and with the X-ray diffraction results. The relative concentration of Fe atoms at A and B sites were obtained from the relative area of the Mössbauer subspectra. The resulting ratio, area (A)/area [B], indicates that these ferrites are not completely inverse and nickel, cobalt and copper ions occupy partially the tetrahedral

Table 1
Crystallite sizes (D) and Mössbauer parameters obtained for different spinel ferrites, at 25 K. δ: Isomer shift (relative to α-Fe); ξ: quadrupole splitting; B_{HF}: magnetic hyperfine field; A: tetrahedral sites; B: octahedral sites.

Sample	D (±1) (nm)	Site	δ (±0.05) mm/s	ξ (±0.05) mm/s	B_{HF} (±0.5) Tesla	Area (%)
Co-ferrite	4	A	0.41	−0.04	48.7	55
		B	0.45	0.03	51.7	45
Cu-ferrite	10	A	0.40	−0.02	49.6	63
		B	0.47	0.02	52.6	37
Ni-ferrite	9	A	0.38	−0.01	50.3	64
		B	0.48	−0.01	54.1	36
(CoNi)-ferrite	4	A	0.40	0.00	49.0	64
		B	0.47	0.03	52.7	36
(CuNi)-ferrite	3	A	0.42	0.01	48.3	63
		B	0.47	0.02	52.2	37
(CoCu)-ferrite	8	A	0.39	−0.02	50.1	61
		B	0.38	0.02	53.4	39

sites, as usually found in nanostructured ferrites [14,23]. At room temperature, the samples presented superparamagnetic relaxation, as indicated by the collapse of the sixth line of the ferrimagnetic Mössbauer spectrum, due to the nanostructural nature of the material.

XPS was used to distinguish the oxidation state of the cations present on the surfaces. However, the analyses of Fe 2p spectra are relatively complex for ferrites. The bivalent Fe $2p_{3/2}$ peak at 709.5 eV and the trivalent Fe $2p_{3/2}$ peak at 711.2 eV are respectively associated to satellite peaks at 715.5 eV and 719.0 eV [24–28]. In the case of our samples the observed Fe $2p_{3/2}$ peaks with binding energies (BE) between 710.7 eV and 711.2 eV, and the associated satellite at around 718.5 eV (Fig. 3), confirm the predominance of Fe^{3+} on the ferrites surface. The observed BE shifts (up to 0.5 eV) can be attributed to the different surroundings of the Fe^{3+} ions in the A and B sites within the ferrite structure. Moreover, the low intensity of the satellite peak could be due to a small fraction of Fe^{2+} present on the surface of the samples. The Ni $2p_{3/2}$ peaks observed between 854.2 eV and 854.6 eV confirm the presence of only Ni^{2+} on the surface [24–29].

The Co 2p and Cu 2p peaks are displayed in Fig. 4. The Co 2p peak suggests the presence of Co^{2+} and Co^{3+} on the surfaces of the ferrites. The analysis takes into account the characteristic Co $2p_{3/2}$ binding energies and the intensity differences between

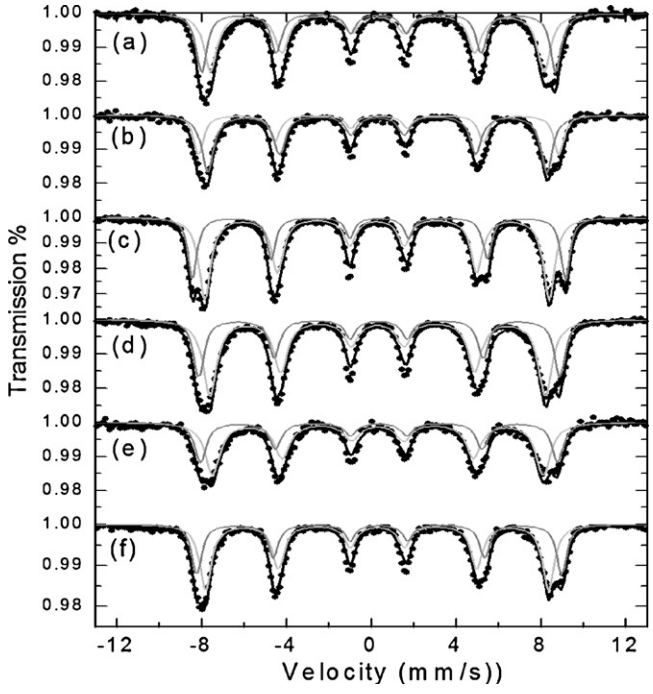

Fig. 2. Mössbauer spectra of the different ferrites at 25 K: Co-ferrite (a), Cu-ferrite (b), Ni-ferrite (c), (CoNi)-ferrite (d), (CuNi)-ferrite (e), (CoCu)-ferrite (f).

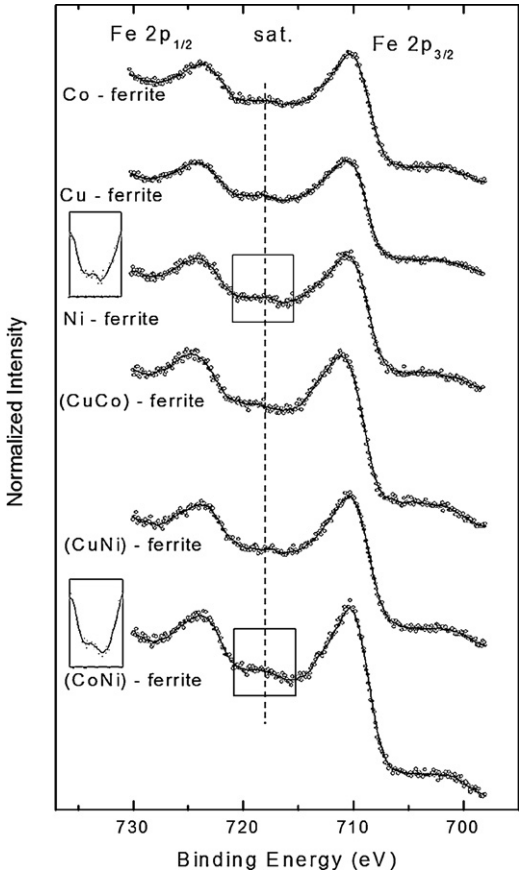

Fig. 3. XPS spectra of the Fe 2p of the spinel ferrites.

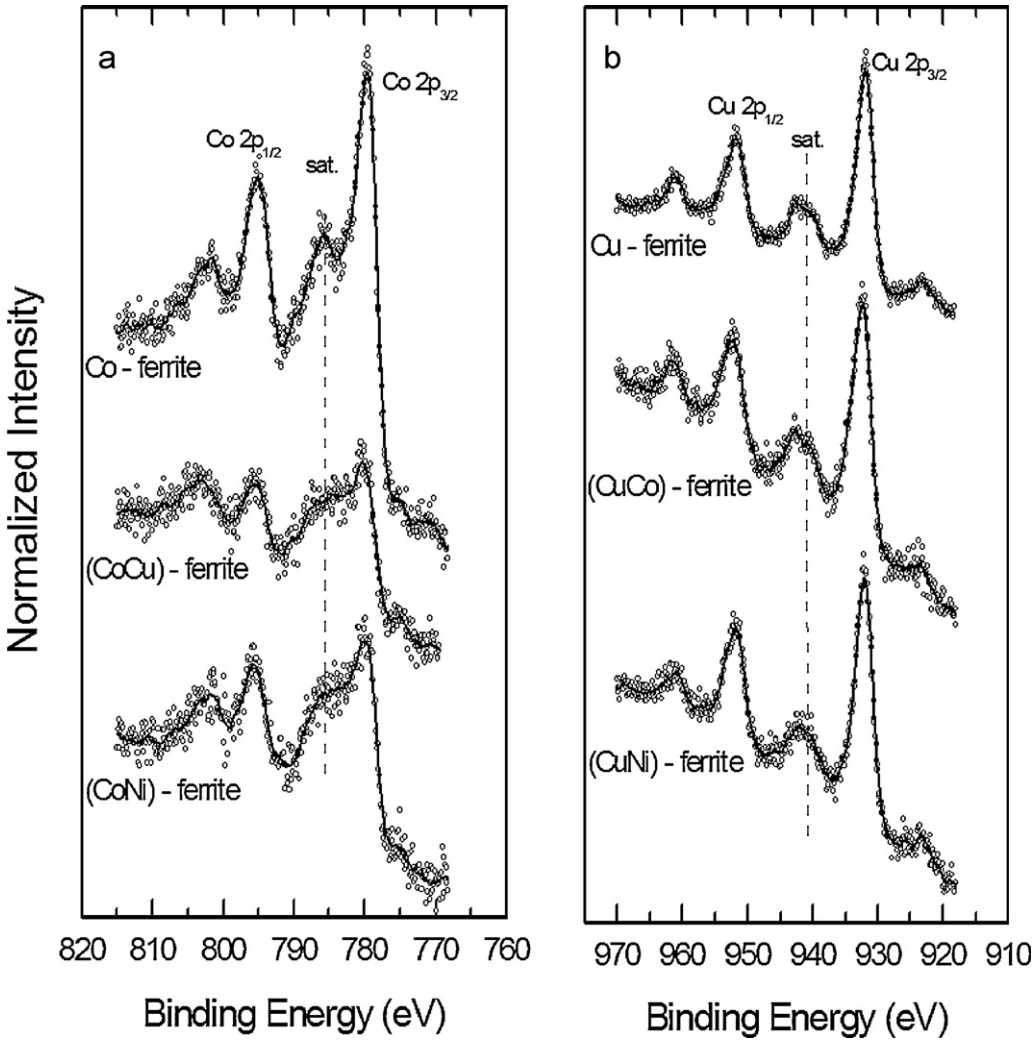

Fig. 4. Co 2p (a) and Cu 2p (b) detailed XP spectra of the spinel ferrites.

the Co $2p_{3/2}$ and its satellite peaks (Fig. 4a). The (CoCu)- and (CoNi)-ferrites exhibit a high intensity satellite peak, a feature associated to Co^{2+} [26,30–34]. In the case of Co-ferrite, the low intensity satellite peak at 786.0 eV indicates the presence of Co^{3+} and Co^{2+} [31–33]. Copper seems to be present also in two oxidation states at the surface of the ferrites. The Cu $2p_{3/2}$ peak centered at 932.4 eV is typical from Cu^{+} and a shake-up satellite situated at 942.0 eV is indicative of the presence of Cu^{2+} [25,26,31]. The relatively low intensity of the satellite peaks and the binding energies observed in all spectra of Cu $2p_{3/2}$ (Fig. 4b) indicate the presence of Cu^{2+} and Cu^{+} on the surface of the Cu-containing samples. Our XPS results are summarized in Table 2.

3.2. Hydrogen peroxide decomposition

These ferrite samples were used as heterogeneous catalysts to promote the hydrogen peroxide decomposition.

$$H_2O_2 \rightarrow H_2O + 0.5O_2 \quad (1)$$

The hydrogen peroxide decomposition is a versatile probe reaction used to investigate the activity of heterogeneous

Table 2
Summarized data of binding energies for the main XPS peaks.

Sample	Fe $2p_{3/2}$	Satellite	Ni $2p_{3/2}$	Satellite	Co $2p_{3/2}$	Satellite	Cu $2p_{3/2}$	Satellite
	Binding energy/eV							
Co-ferrite	710.7	718.0	–	–	780.0	786.0	–	–
Cu-ferrite	710.8	718.0	–	–	–	–	932.0	942.3
Ni-ferrite	710.6	718.7	854.4	860.8	–	–	–	–
(CoCu)-ferrite	711.1	718.6	–	–	780.2	785.5	932.4	942.0
(NiCu)-ferrite	710.8	718.2	854.2	860.7	–	–	932.4	942.0
(CoNi)-ferrite	710.8	717.5	854.6	861.1	780.1	785.1	–	–

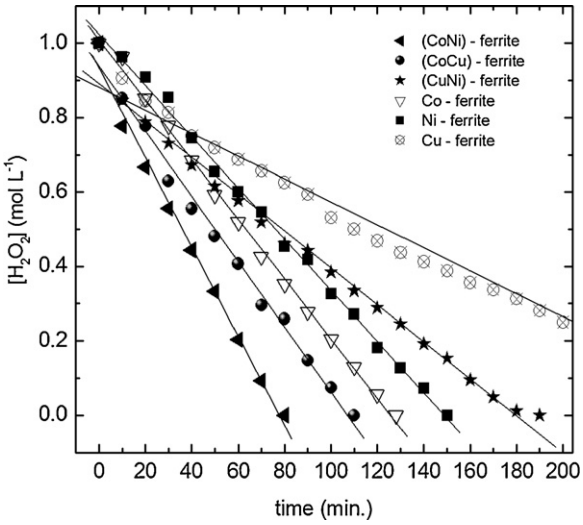

Fig. 5. Hydrogen peroxide decomposition in the presence of different spinel ferrites.

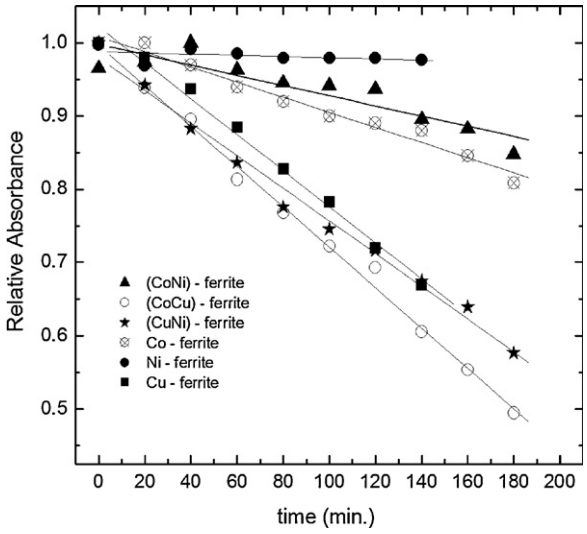

Fig. 6. Methylene blue oxidation in the presence the different spinel ferrites.

systems towards the Fenton chemistry [35,36]. Results obtained from peroxide decomposition with different ferrites are shown in Fig. 5.

The decomposition plots exhibit a linear behavior. Similar kinetic behavior has been observed before for other ferrites, e.g. [36,37]. Based on this, it can be said that the reaction has a pseudo zeroth order dependence on the H_2O_2 concentration, $V_{dec} = k\text{-}_{dec}[H_2O_2]^0$. Hence, the reaction rates can be estimated from the linear fit of the decomposition plots. The ferrites which contain Co, i.e., Co-, (CoCu)- and (CoNi)-ferrites, show very high activity, with constant reaction rates of 0.48, 0.52 and 0.72 mmol min^{-1}, respectively, and therefore the peroxide is totally consumed after 2 min of reaction. It is well established in the literature that Co^{2+} plays an important role in the hydrogen peroxide decomposition [4]. The small difference in the activity of the Co-ferrite compared to that of (CoCu)- and (CoNi)-ferrites may be due to the presence of higher concentration of Co^{3+} on the Co-ferrite surface, as shown by XPS.

The Ni ferrite exhibits low activity in the decomposition of hydrogen peroxide with constant rate of 0.07 mmol min^{-1}. However the presence of Cu in the Ni-ferrite increases the constant rate to 0.10 mmol min^{-1} and the Cu-ferrite showed a reaction rate of 0.18 mmol min^{-1}. This activity of Cu-containing ferrites can be explained by the presence of the redox pair Cu^+/Cu^{2+} at the surface [2,10].

3.3. Oxidation of methylene blue

Oxidation studies were carried out with dye methylene blue and H_2O_2 as oxidized agent. The oxidation of the methylene blue was monitored by discoloration, which is related to the first oxidation steps to produce non-colored intermediates according to Eq. (2):

$$\underline{\text{Discoloration}}\text{Dye} + H_2O_2 \rightarrow \text{non-coloredintermediates} \quad (2)$$

$$\underline{\text{Mineralization}}\text{intermediates} + H_2O_2 \rightarrow CO_2/H_2O \quad (3)$$

The discoloration activities obtained by different ferrites are shown in Fig. 6. From this figure, it is possible to observe that under the conditions employed no significant discoloration was produced by nickel ferrite with constant rate of 8×10^{-5} min^{-1}. It was also observed an increase in the discoloration activity with the presence of Co in the ferrite structure of (NiCo)-ferrite and Co-ferrite, with constant rate of 5 and 6×10^{-4} min^{-1}, respectively. However, when Cu is introduced in the structure of the spinel to form Cu-, (CuNi)- and (CoCu)-ferrite, the constant rate of discoloration increases respectively to 1.6, 2.4 and 2.7×10^{-3} min^{-1}. It was possible to observe a discoloration of 50% in 180 min of reaction in the case of (CoCu)-ferrite. This behavior could be related to the presence of Cu, since Cu changes significantly the electronic structure of the ferrite [11], increasing the electron availability and therefore the oxidation of the organic compounds. These results suggest distinct redox properties of Cu in both reactions with H_2O_2, decomposition and oxidation of organics, especially in the case of (CoCu)-ferrite.

3.4. The reaction mechanism

The hydrogen peroxide decomposition has been proposed in the literature [38] to take place by the formation of radicals from H_2O_2 that decompose with partially reduced surface species, for example, Fe^{2+}, according to the Haber–Weiss mechanism:

$$Fe^{2+}{}_{surf} + H_2O_2 \rightarrow Fe^{3+}{}_{surf} + {}^{\bullet}OH + OH^- \quad (4)$$

The $HO^{\bullet}$ radicals can react by two competitive pathways: (i) with H_2O_2 to produce the peroxide radical $HOO^{\bullet}$ which reacts with Fe^{3+} surface species to produce O_2 (Eqs. (5) and (6)), and (ii) with organic molecules, e.g. methylene blue, in an oxidation process.

$$H_2O_2 + {}^{\bullet}OH \rightarrow H_2O + {}^{\bullet}OOH \quad (5)$$

$$Fe^{3+}{}_{surf} + {}^{\bullet}OOH \rightarrow Fe^{2+}{}_{surf} + H^+ + O_2 \quad (6)$$

Our results show that Ni ferrites presented no activity for both reactions, peroxide decomposition and oxidation of methylene blue. On the other hand, when Ni is substituted in the ferrite structure by Co and Cu it is observed an increase in the activity of peroxide decomposition and methylene blue oxidation.

Although the effect of these metals is not clear, several points can be raised in order to discuss their role in the reaction. Regarding nickel, it can be considered that only the Ni^{2+} species are stable, and for this reason they cannot initiate the radicalar reaction according to Eq. (4). On the other hand, cobalt and copper exhibit the redox pairs Co^{2+}/Co^{3+} and Cu^{+}/Cu^{2+} which can also produce radicals according to reactions (7) and (8):

$$Co^{2+}{}_{surf} + H_2O_2 \rightarrow Co^{3+}{}_{surf} + OH^- + {}^{\bullet}OH \quad (7)$$

$$Cu^{+}{}_{surf} + H_2O_2 \rightarrow Cu^{2+}{}_{surf} + OH^- + {}^{\bullet}OH \quad (8)$$

In addition, if M^{3+}, present in the ferrite, is reduced during the decomposition of hydrogen peroxide as shown in Eq. (6) there is the possibility to regenerate the Co^{2+}, Cu^{+} and, even Fe^{2+}, as shown by XPS analyses, which can make the process catalytic.

However, in the Fenton reaction with copper, the complex formed between H_2O_2 and the Cu is very stable compared to Fenton reactions with iron or cobalt. So, the activated species in the reaction with copper can be ${}^{\bullet}OH$ or Cu^{3+} and the reaction can be 3 times faster [39]. For this reason, the reaction with Cu ferrites can favor the H_2O_2 decomposition to form O_2 in the competitive reaction compared to the oxidation of organic reactions.

4. Conclusions

Nanostructured spinel ferrites were synthesized via co-precipitation method and characterized with several techniques in order to know the structural aspects of the samples, and aiming to employ these materials as catalysts in the oxidation of synthetic dyes, e.g. methylene blue. The performance of the ferrites is understood considering the oxidation states of the elements at the surface of the ferrites. We observed that the presence of cobalt ions is crucial for a systematic efficiency of the catalyst in H_2O_2 decomposition. In contrast, the Cu-containing ferrites presented the better performance in methylene blue oxidation, which can be attributed to the different redox properties of Cu and the easy availability of electrons to participate in the oxidation of organic compounds. The studied ferrites are a promising potential candidate for the development of new materials to be used in larger scales oxidation processes involving organic substrates.

Acknowledgments

The authors are grateful to Conselho Nacional de Desenvolvimento Científico e Tecnológico – CNPq, Fundação de Amparo à Pesquisa do Estado de Minas Gerais – FAPEMIG, and Coordenação de Aperfeiçoamento de Pessoal de Nível Superior – CAPES, for the financial support, and to Comissão Nacional de Energia Nuclear – CNEN for the use of their laboratory facilities.

References

[1] T.L.P. Dantas, V.P. Mendonça, H.J. José, A.E. Rodrigues, R.F.P.M. Moreira, Treatment of textile wastewater by heterogeneous Fenton process using a new composite Fe_2O_3/carbon, Chem. Eng. J. 118 (2006) 77–82.
[2] P. Baldrian, V. Merhautová, J. Gabriel, F. Nerud, P. Stopka, M. Hrubý, M.J. Benes, Decolorization of synthetic dyes by hydrogen peroxide with heterogeneous catalysis by mixed iron oxides, Appl. Catal. B 66 (2006) 258–264.
[3] F. Magalhães, M.C. Pereira, S.E.C. Botrel, J.D. Fabris, W.A.A. Macedo, R. Mendonça, R.M. Lago, L.C.A. Oliveira, Cr-containing magnetites $Fe_{3-x}Cr_xO_4$: the role of Cr^{3+} and Fe^{2+} on the stability and reactivity towards H_2O_2 reactions, Appl. Catal. A 332 (2007) 115–123.
[4] R.C.C. Costa, M.F.F. Lelis, L.C.A. Oliveira, J.D. Fabris, J.D. Ardisson, R.R.V.A. Rios, C.N. Silva, R.M. Lago, Remarkable effect of Co and Mn on the activity of $Fe_{3-x}M_xO_4$ promoted oxidation of organic contaminants in aqueous medium with H_2O_2, Catal. Commun. 4 (2003) 525–529.
[5] K. Omata, T. Takada, S. Kasahara, M. Yamada, Active site substituted cobalt spinel oxide for selective oxidation of CO/H-2. Part 2, Appl. Catal. A: Gen. 146 (1996) 255–267.
[6] M. Florea, M. Alifanti, V.I. Parvulescu, D. Mihaila-Tarabasanu, L. Diamandescu, M. Feder, C. Negrila, L. Frunza, Total oxidation of toluene on ferrite-type catalysts, Catal. Today 141 (2009) 361–366.
[7] B.D. Cullity, Introduction to Magnetic Materials, Addson-Wesley Publ. Company, London, 1972.
[8] C.W. Chen, Magnetism and Metallurgy of Soft Magnetic Materials, Dover Public Inc., New York, 1986.
[9] J.P. Jacobs, A. Maltha, J.G.H. Reitjes, J. Drimal, V. Ponec, H.H. Brongersma, The surface of catalytically active spinels, J. Catal. 47 (1994) 294–300.
[10] C.G. Ramankutty, S. Sugunan, Surface properties and catalytic activity of ferrospinels of nickel, cobalt and copper, prepared by soft chemical methods, Appl. Catal. A 218 (2001) 39–51.
[11] C.G. Ramankutty, S. Sugunan, B. Thomas, Study of cyclohexagonal decomposition reaction over the ferrospinels, $A(1-x)Cu(x)Fe(2)O(4)$ (A = Ni or Co and $x = 0$, 0.3, 0.5, 0.7 and 1) prepared by soft chemical methods, J. Mol. Catal. A 187 (2002) 105–117.
[12] J.S. Kim, J.R. Ahn, Characterization of wet processed (Ni, Zn)-ferrites for CO_2 decomposition, J. Mater. Sci. 36 (2001) 4813–4816.
[13] A.S. Albuquerque, J.D. Ardisson, W.A.A. Macedo, M.C.M. Alves, Nano-sized powders of NiZn ferrite: synthesis, structure, and magnetism, J. Appl. Phys. 87 (2000) 4352–4357.
[14] J.E. Tasca, C.E. Quincoces, A. Lavat, A.M. Alvarez, M.G. González, Preparation and characterization of $CuFe_2O_4$ bulk catalysts, Ceram. Int. 37 (2011) 803–812.
[15] T. Mathew, S. Shylesh, B.M. Devassy, M. Vijayaraj, C.V.V. Satyanarayana, B.S. Rao, C.S. Gopinath, Selective production of orthoalkyl phenols on $Cu_{0.5}Co_{0.5}Fe_2O_4$: a study of catalysis and characterization, Appl. Catal. A: Gen. 273 (2004) 35–45.
[16] X. Tan, Y. Zhao, G. Li, C. Hu, Effect of calcination temperatura on the structure and hydroxylation activity of $Ni_{0.5}Cu_{0.5}Fe_2O_4$ nanoparticles, Appl. Surf. Sci. 257 (2011) 6256–6263.
[17] C. Sub Lee, C. Young Lee, Superexchange interactions in $Ni_{0.5}Co_{0.5}$-Fe_2O_4, J. Appl. Phys. 79 (1996) 5710–5712.
[18] M.A.G. Soler, E.C.D. Lima, S.W. da Silva, T.F.O. Melo, A.C.M. Pimenta, J.P. Sinnecker, R.B. Azevedo, V.K. Garg, A.C. Oliveira, M.A. Novak, P.C. Morais, Aging investigation of cobalt ferrite nanoparticles in low pH magnetic fluid, Langmuir 23 (2007) 9611–9617.
[19] M.M. El-Okr, M.A. Salem, M.S. Salim, R.M. El-Okr, M. Ashoush, H.M. Talaat, Synthesis of cobalt ferrite nano-particles and their magnetic characterization, J. Magn. Magn. Mater. 323 (2011) 920–926.
[20] K. Velmurugan, V.S.K. Venkatachalapathy, S. Sendhilnathan, Synthesis of nickel zinc iron nanoparticles by coprecipitation technique, Mater. Res. 13 (2010) http://dx.doi.org/10.1590/S1516-14392010000300005.
[21] A.M. Banerjee, M.R. Pai, S.S. Meena, A.K. Tripathi, S.R. Bharadwaj, Catalytic activities of cobalt, nickel and copper ferrospinels for sulfuric acid decomposition: the high temperature step in the sulfur based thermochemical water splitting cycles, Int. J. Hydrogen Energy 36 (2011) 4768–4780.

[22] M. Siddique, N.M. Butt, Effect of particle size on degree of inversion in ferrites investigated by Mössbauer spectroscopy, Phys. B: Condens. Matter 405 (2010) 4211–4215.
[23] G. Salazar-Alvarez, R.T. Olsson, J. Sort, W.A.A. Macedo, J.D. Ardisson, M.D. Baró, U.W. Gedde, J. Nogués, Enhanced coercivity in Co-rich near-stoichiometric $CoFe_{3-x}O_4$ + delta nanoparticels prepared in large batches, Chem. Mater. 19 (2007) 4957–4963.
[24] V.K. Mittal, P. Chandramohan, S. Bera, M.P. Srinivasan, S. Velmurugan, S.V. Narasimhan, Cation distribution in $Ni_xMg_{1-x}Fe_2O_4$ studied by XPS and Mossbauer spectroscopy, Solid State Commun. 137 (2006) 6–10.
[25] T. Yamashita, P.A. Hayes, Analysis of XPS spectra of Fe^{2+} and Fe^{3+} ions in oxide materials, Appl. Surf. Sci. 254 (2008) 2441–2449.
[26] M. Vijayaraj, C.S. Gopinath, On the active spacer and stabilizer role of Zn in $Cu_{1-x}Zn_xFe_2O_4$ in the selective mono-N-methylation of aniline: XPS and catalysis study, J. Catal. 241 (2006) 83–95.
[27] T. Mathew, N.R. Shiju, V.V. Bokade, B.S. Rao, C.S. Gopinath, Selective catalytic synthesis of 2-ethil phenol over $Cu_{1-x}Co_xFe_2O_4$-kinetics, catalysis and XPS aspects, Catal. Lett. 94 (2004) 223–236.
[28] R. Muñoz, M. Martos, C.M. Rotaru, H. Beltran, E. Cordoncillo, P. Escribano, Influence of the precursors on the formation and properties of the $Fe_xCr_{2-x}O_3$ solid solution, J. Eur. Ceram. Soc. 26 (2006) 1363–1370.
[29] V.K. Mittal, S. Bera, R. Nithya, M.P. Srinivasan, S. Velmurugan, S.V. Narasimhan, Solid state synthesis of Mg–Ni ferrite and charaterization by XRD and XPS, J. Nucl. Mater. 335 (2004) 302–310.
[30] X. Yang, X. Wang, Z. Zhang, Electrochemical properties of submicron cobalt ferrite through a co-precipitation method, J. Cryst. Growth 277 (2005) 467–470.
[31] T. Mathew, N.R. Shiju, K. Sreekumar, B.S. Rao, C.S. Gopinath, Cu–Co synergism in $Cu_{1-x}Co_xFe_2O_4$ – catalysis and XPS aspects, J. Catal. 210 (2002) 405–417.
[32] D.V. Cesar, C.A. Perez, M. Schmal, V.M.M. Salim, Quantitative XPS analysis of silica-supported Cu–Co oxides, Appl. Surf. Sci. 157 (2000) 159–166.
[33] S.C. Petitto, M.A. Langell, Cu_2O(1 1 0) formation on Co_3O_4(1 1 0) induced by copper impurity segregation, Surf. Sci. 599 (2005) 27–40.
[34] P. Stefanov, I. Avramova, D. Stoichev, N. Radic, B. Grbic, T.S. Marinova, Characterization and catalytic activity of Cu–Co spinel thin films catalysts, Appl. Surf. Sci. 245 (2005) 65–72.
[35] R.C.C. Costa, M.F.F. Lelis, L.C.A. Oliveira, J.D. Fabris, J.D. Ardisson, R.R.V.A. Rios, C.N. Silva, R.M. Lago, Novel active heterogeneous Fenton system based on $Fe_{3-x}M_xO_4$ (Fe, Co, Mn, Ni): The role of M^{2+} species on the reactivity towards H_2O_2 reactions, J. Hazard. Mater. B 129 (2006) 171–178.
[36] R.C.C. Costa, F.C.C. Moura, J.D. Ardisson, J.D. Fabris, R.M. Lago, Highly active heterogeneous Fenton-like systems based on Fe-0/Fe_3O_4 composites prepared by controlled reduction of iron oxides, Appl. Catal. B 83 (2008) 131–139.
[37] F.C.C. Moura, M.H. Araujo, J.D. Ardisson, W.A.A. Macedo, A.S. Albuquerque, R.M. Lago, Investigation of the solid state reaction of $LaMnO_3$ with Fe-0 and its effect on the catalytic reactions with H_2O_2, J. Braz. Chem. Soc. 18 (2007) 322–329.
[38] W.P. Kwan, B.M. Voelker, Rates of hydroxyl radical generation and organic compound oxidation in mineral-catalyzed Fenton-like systems, Environ. Sci. Technol. 37 (2003) 1150–1158.
[39] P. Wardman, L.P. Candeias, Fenton chemistry: an introduction, Radiat. Res. 145 (1996) 523–531.